Supplementary Materials

Ultralow thermal conductivity via weak interactions in PbSe/PbTe monolayer heterostructure for thermoelectric design

Ruihao Tan[1], Kaiwang Zhang[1,*], Yue-Wen Fang[2,*]

[1]School of Physics and Optoelectronics, Xiangtan University, Xiangtan 411105, Hunan, China.
[2]Centro de Física de Materiales (CFM-MPC), CSIC-UPV/EHU, San Sebastián 20018, Spain.

[*]**Correspondence to:** Prof. Kaiwang Zhang, School of Physics and Optoelectronics, Xiangtan University, Xiangtan 411105, Hunan, China. E-mail: kwzhang@xtu.edu.cn; Prof. Yue-Wen Fang, Centro de Física de Materiales (CFM-MPC), CSIC-UPV/EHU, San Sebastián 20018, Spain. E-mail: yuewen.fang@ehu.eus

I. Convergence Test Using ShengBTE

To ensure the accuracy of lattice thermal conductivity calculations, **q**-point mesh convergence tests were carried out using ShengBTE and FourPhonon for both three-phonon (Supplementary Figure 1) and four-phonon (Supplementary Figure 2). The convergence threshold was defined as a variation of less than 0.1 W/mK.

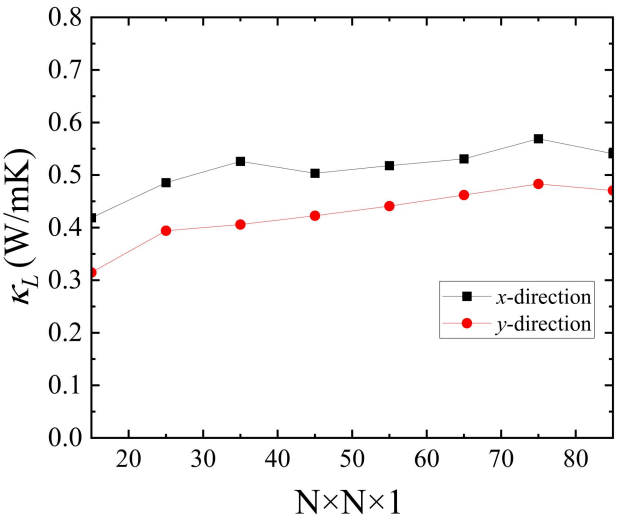

Supplementary Figure 1. Convergence behavior of lattice thermal conductivity in PbSe/PbTe monolayer heterostructure under the three-phonon scattering model, evaluated with varying **q**-point meshes and a smearing width of 0.1.

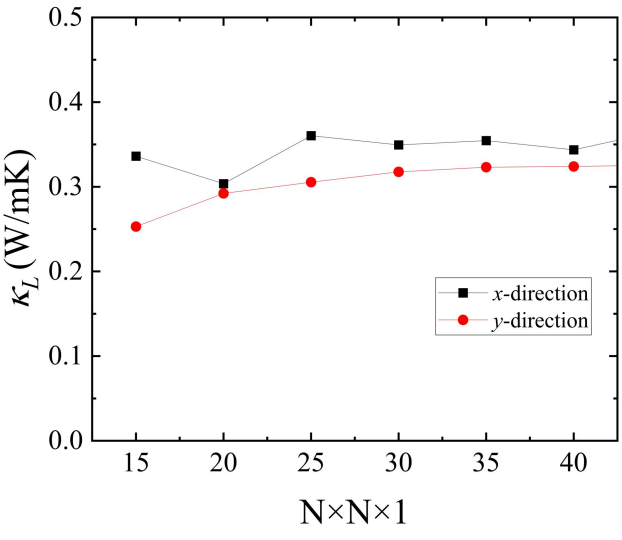

Supplementary Figure 2. Convergence behavior of lattice thermal conductivity in PbSe/PbTe monolayer heterostructure under the Four-phonon scattering model, evaluated with varying **q**-point meshes and a smearing width of 0.1.

II. Variation of CBM/VBM under Strain

As shown in Supplementary Figure 3, the electron and hole carrier mobilities were evaluated using the deformation potential theory, considering the strain-induced shifts in the conduction band minimum (CBM) and valence band maximum (VBM).

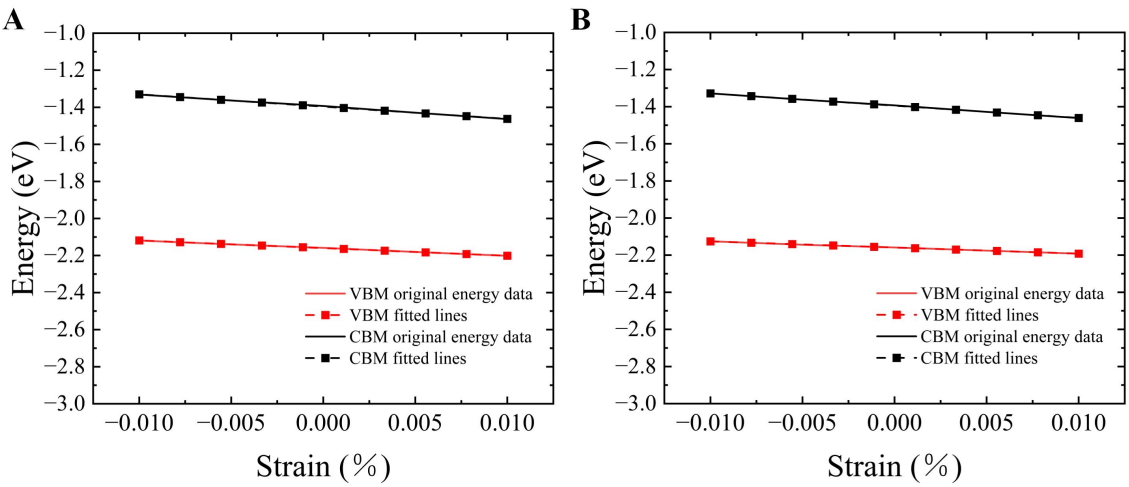

Supplementary Figure 3. The variation of the total energy under uniaxial strain (from -1% to 1%) for the PbSe/PbTe monolayer heterostructure is calculated using the Perdew-Burke-Ernzerhof (PBE) functional. The left and right panels correspond to strain applied along the (A) *x*-direction and (B) *y*-direction, respectively. The red and black curves represent the original energy data and the fitted curves of the VBM and CBM under different strains, which are used to extract the deformation potential constant (*E*).

III. Discussion of MTP potential and accuracy

Moment Tensor Potential (MTP) is based on the locality principle, where the total energy of a system with N atoms is given as a sum over atomic neighborhood contributions[1]:

$$E = E^{\mathrm{MTP}} = \sum_i V(u_i) \qquad (1)$$

Here, $V(u_i)$ represents the energy contribution from the neighborhood of atom i. Two atoms are considered neighbors if their separation is less than a defined cutoff distance R_{cut}. In our case, R_{cut} = 5 Å was used. The neighborhood u_{i} of atom i includes the positions and types of all its neighbors[1]:

$$u_i = \left(\{r_{i1}, z_i, z_1\} \ldots, \{r_{ij}, z_i, z_j\} \ldots, \{r_i N_{neigh}, z_i, z N_{neigh}\}\right) \qquad (2)$$

In this context, r_{ij}, z_i, z_j , and N_{neigh} denote the vector between atoms, the type of the central atom, the type of neighboring atoms, and the count of neighboring atoms, respectively. For a given atomic configuration, its energy contribution is represented as: $V(u_i) = \sum_\alpha \xi_\alpha B_\alpha(u_i)$ where B_α are the basis functions and ξ_α are tunable parameters within the machine-learned interatomic potential (MLIP). A scalar quantity is then constructed by combining all possible contractions of moment tensor descriptors through these basis functions. A scalar based on basis functions constructed from all possible contractions of moment tensor descriptors is generated as follows[1]:

$$M_{\mu,\nu}(u) = \sum_{j=1}^{N_i^{\mathrm{neigh}}} f_\mu(|r_{ij}|, z_i, z_j)(r_{ij})^{\otimes \nu} \qquad (3)$$

Here, the radial function f_μ depends on the interatomic distance and atomic types, and is given by[1]:

$$f_\mu(|r_{ij}|, z_i, z_j) = \sum_\beta c_{\mu\beta}^{(z_i, z_j)} \phi_\beta(|r_{ij}|) \chi(R_{\mathrm{cut}} - |r_{ij}|) \qquad (4)$$

where ϕ_β are radial basis functions, χ is a cutoff smoothing function, and $c_{\mu\beta}$ are learnable coefficients.

To verify the applicability of the MLIP used in this study, namely, the MTP, for the PbSe/PbTe monolayer heterostructure, we present key performance indicators and error statistics from the training process. The MTP model achieved a mean absolute error (MAE) of 0.00040 eV/atom for atomic energies, with a maximum deviation of 0.00192 eV/atom and a root mean square error (RMSE) of 0.00059 eV/atom. For atomic forces, the average error was 0.0154 eV/Å, with an RMSE of 0.0310 eV/Å. The relative error

in force fluctuations is only 8.65%, well below the commonly accepted threshold of 15% for reliable atomic simulations, indicating good accuracy and predictive capability.[2]

To further validate the reliability of the MTP potential in describing the phonon transport properties of the PbSe/PbTe monolayer heterostructure, we compared the phonon dispersion curves calculated using MTP with those obtained from density functional theory (DFT). As shown in Supplementary Figure 4, the two sets of results are in excellent agreement, demonstrating that the MTP model accurately captures the lattice dynamics of the heterostructure. This confirms the robustness of MTP in predicting phonon transport properties with high fidelity.[3]

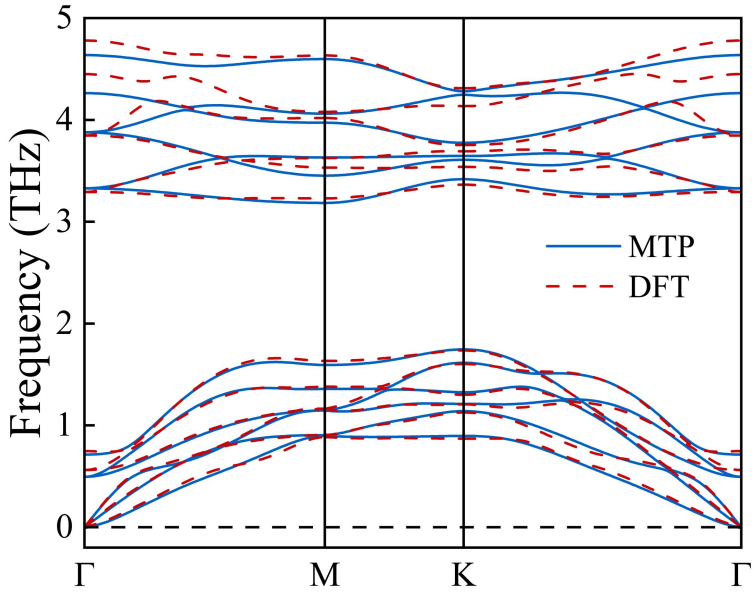

Supplementary Figure 4. Phonon dispersion curves of PbSe/PbTe monolayer heterostructure calculated using the finite displacement method (red dashed lines) and the machine-learned moment tensor potential (MTP) approach (blue solid lines).

IV. Anisotropic Displacement Parameter

Our anisotropic displacement parameter (ADP) calculations are derived from the thermal displacement and mean square displacement (MSD) calculations. Specifically, thermal displacement refers to the vibration of atoms within the lattice caused by temperature changes, and MSD is used to quantify the average deviation of atoms from their equilibrium positions.

For the calculation of MSD, we first used Phonopy software to compute the thermal vibrations of atoms at different temperatures. MSD reflects the intensity of atomic displacement due to thermal vibrations and is calculated using:

$$\langle u^2 \rangle = \langle \Delta r^2 \rangle = \frac{1}{N} \sum_{i=1}^{N} \langle \left(\mathbf{r}_i(t) - \mathbf{r}_i(0) \right)^2 \rangle, \quad (5)$$

where $\mathbf{r}_i(t)$ represents the displacement of atom i at time t, and $\mathbf{r}_i(0)$ is the equilibrium position of the atom. By calculating the MSD, we can accurately describe the vibration amplitude of atoms in the crystal along different directions.

Furthermore, the ADPs reflect the intensity of atomic vibrations along different directions. Using the MSD results calculated by Phonopy, we further derived the ADPs along each direction. The relationship between ADP and MSD can be expressed as:

$$\langle u^2 \rangle = \langle u_x^2 \rangle + \langle u_y^2 \rangle + \langle u_z^2 \rangle, \quad (6)$$

where $\langle u_x^2 \rangle$, $\langle u_y^2 \rangle$, and $\langle u_z^2 \rangle$ represent the MSD values along the *x*, *y*, and *z* directions, respectively.

It is worth noting that ADP not only reflects the intensity of atomic vibrations but also indirectly indicates the strength of atomic bonds. When the chemical bonds between atoms are stronger, the amplitude of atomic vibrations is smaller, leading to a lower ADP value. Conversely, when the bonds are weaker, the atomic vibrations are larger, resulting in a higher ADP value. Therefore, ADP can serve as an indirect indicator of bond strength within a material. In our study, by analyzing the distribution of ADP values across different atoms, we can identify regions of stronger or weaker bonding.

V. The inverse calculation process of the Sebeck coefficient and the derivation of related formulas

1. Carrier Concentration and Fermi Level Relationship

Using the 2D degenerate Fermi gas approximation, the relationship between carrier concentration n_{2D} and the Fermi level E_F relative to the CBM E_C is given by [4]:

$$n_{2D} = \frac{g_s g_v m^*}{2\pi\hbar^2}(E_F - E_C) \tag{7}$$

where:

n_{2D} is the carrier concentration in m^{-2},

$g_s = 2$ is the spin degeneracy,

$g_v = 1$ is the valley degeneracy (assuming a single valley material),

m^* is the effective mass in units of electron mass m_0 ($m^* \approx 0.5m_0$),

$\hbar = 1.055\times10^{-34}\,\mathrm{J\bullet s}$ is the reduced Planck's constant,

E_F is the Fermi level, and

E_C is the conduction band minimum.

By rearranging the equation, we can obtain the Fermi level relative to the conduction band edge:

$$E_F - E_C = \frac{2\pi\hbar^2 n_{2D}}{g_s g_v m^*} \tag{8}$$

2. Reverse Calculation Results

Using the values from Figure 13B ($n_{2D} = 10^{12}\,\mathrm{cm}^{-2} = 10^{16}\,\mathrm{m}^{-2}$, $m^* = 0.5m_0$), we can calculate the Fermi level relative to the conduction band edge:

$$E_F - E_C = \frac{2\pi(1.055\times10^{-34})^2(1\times10^{16})}{2\times1\times(0.5\times9.11\times10^{-31})} \tag{9}$$

This gives:

$$E_F - E_C \approx 3.8\times10^{-21}\,\mathrm{J} \approx 0.02\,\mathrm{eV} \tag{10}$$

Thus, the Fermi level is approximately 0.02 eV above the conduction band edge.

3. Seebeck Coefficient Calculation

The general form of the Mott relation for the Seebeck coefficient (S) is [5]:

$$S = -\frac{\pi^2 k_B^2 T}{3e}\left[\frac{d\ln\sigma(E)}{dE}\right]_{E=E_F}, \tag{11}$$

where $\sigma(E)$ is the energy-dependent electrical conductivity.

Simplification under Specific Assumptions

The simplified form:

$$S = \frac{\pi^2 k_B^2 T}{3e(E_F - E_C)} \tag{12}$$

is derived under the following assumptions:

1. Parabolic Band Approximation

The electron density of states $g(E)$ follows $g(E) \propto \sqrt{E - E_C}$ (valid for free electrons or near the CBM E_C).

2. Linearized Energy Dependence

The conductivity $\sigma(E)$ is linear in energy:

$$\sigma(E) \propto (E - E_C) \quad \Rightarrow \quad \frac{d \ln \sigma(E)}{dE} = \frac{1}{E_F - E_C} \tag{13}$$

3. Elastic Scattering Dominance

The relaxation time τ is energy-independent (e.g., impurity scattering). If $\tau \propto E^r$, the formula modifies to:

$$S = \frac{\pi^2 k_B^2 T}{3e} \left(\frac{r+1}{E_F - E_C} \right) \tag{14}$$

4. Non-Degenerate Limit

The Fermi level E_F lies sufficiently below E_C (for semiconductors) or above (for metals), i.e., $|E_F - E_C| \gg k_B T$.

Using Mott's formula for the Seebeck coefficient:

$$S = \frac{\pi^2 k_B^2 T}{3e(E_F - E_C)} \tag{15}$$

Substituting the known values: $k_B = 1.381 \times 10^{-23}\,\text{J/K}$ (Boltzmann constant), $T = 300\text{K}$ (temperature), $e = 1.602 \times 10^{-19}\,\text{C}$ (electron charge), $E_F - E_C = 0.02\text{eV} = 3.2 \times 10^{-20}\,\text{J}$,

We obtain:

$$S = \frac{\pi^2 (1.381 \times 10^{-23})^2 \times 300}{3(1.602 \times 10^{-19}) \times 3.2 \times 10^{-20}} \approx 1.35 \times 10^{-3}\,\text{V/K} = 1350\,\mu\text{V/K}$$

This result is in excellent agreement with our first-principles calculation results ($S \approx 1.3\text{mV/K}$ to 1.4mV/K) and confirms that the high Seebeck coefficient arises from

the close proximity of the Fermi level to the conduction band edge, leading to the dominance of high-energy carriers in transport.

VI. Phonon Part

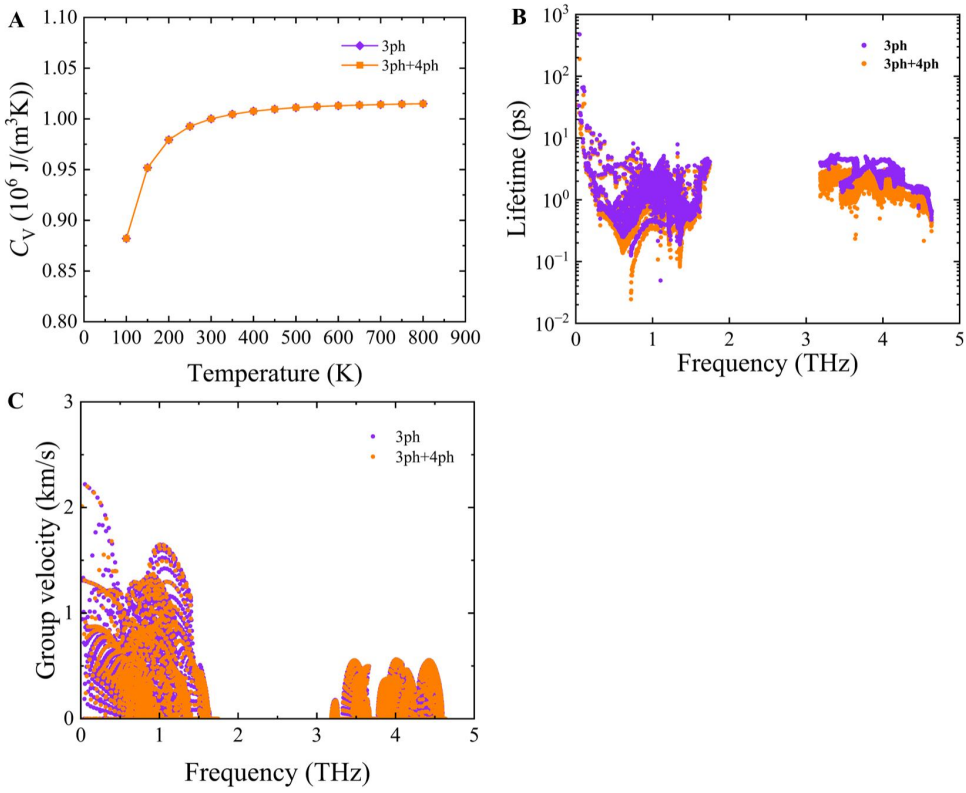

Supplementary Figure 5. For the calculated PbSe/PbTe monolayer heterostructure under three-phonon and four-phonon processes: (A) The variation of specific heat capacity C_v with temperature. (B) Phonon lifetime. (C) Phonon group velocity.

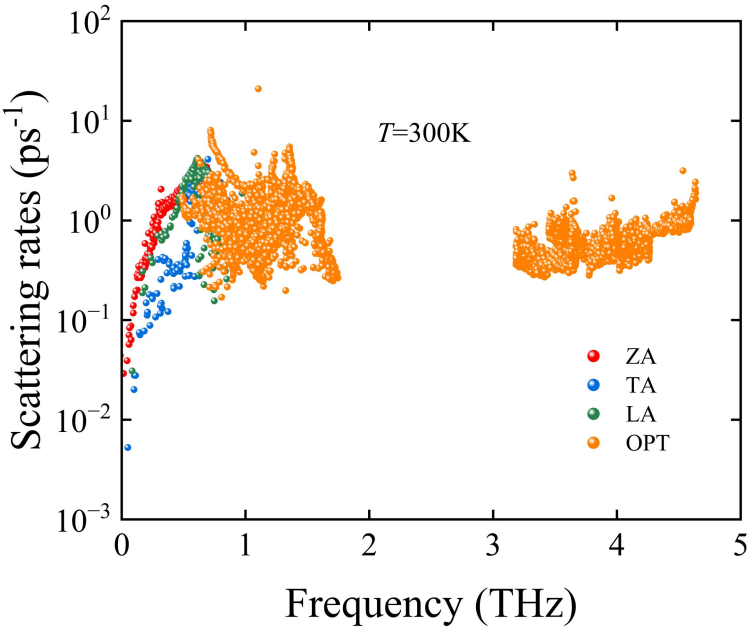

Supplementary Figure 6. Total phonon scattering rates of each mode as a function of frequency at 300 K under the four-phonon scattering model.

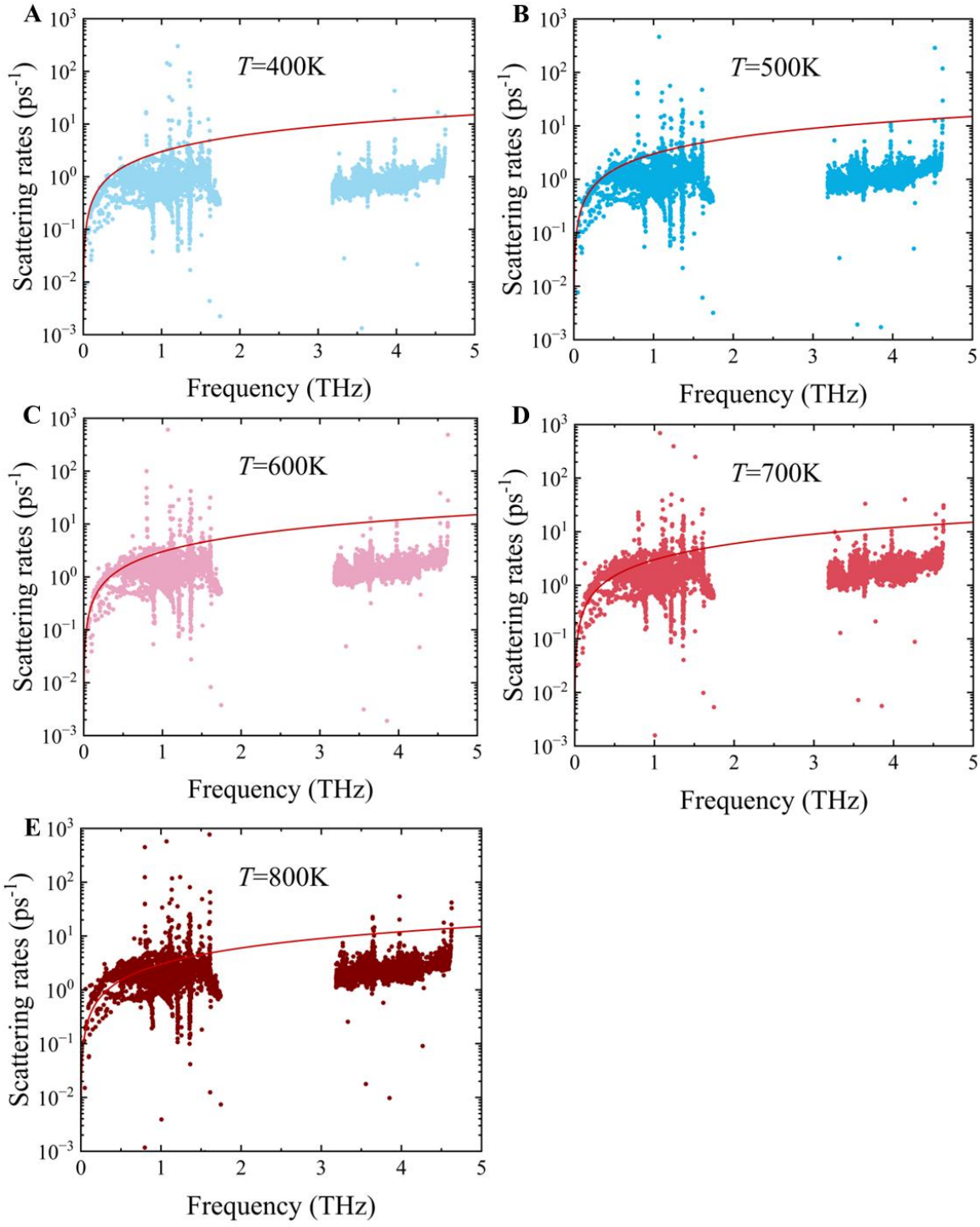

Supplementary Figure 7. Frequency-dependent total scattering rates of the PbSe/PbTe monolayer heterostructure calculated under the four-phonon scattering model in the temperature range of 400 K to 800 K. The red line represents $1/\tau_{ph} = \omega_{ph}/2\pi$.

VII. Band Gap of PbSe/PbTe monolayer heterostructure

As shown in Supplementary Table 1, the electronic band structures were computed using both the Perdew-Burke-Ernzerhof (PBE) and Heyd–Scuseria–Ernzerhof (HSE06) functionals to accurately determine the band gap.

Supplementary Table 1. Band gap values calculated using PBE, PBE+SOC, HSE06, and HSE06+SOC methods for the PbSe/PbTe monolayer heterostructure, with comparison to previously reported results.

Material	Band gap (eV)			
	PBE	PBE+SOC	HSE06	HSE06+SOC
PbSe/PbTe	0.77	0.53	1.25	1.05

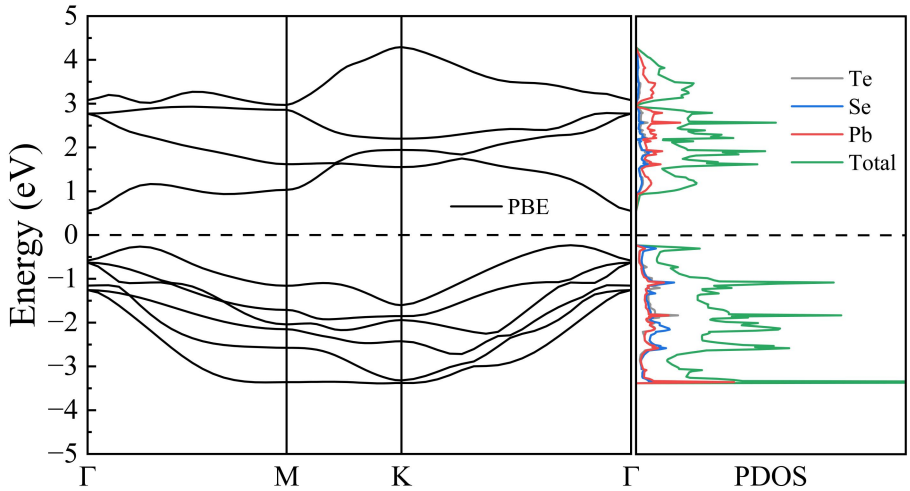

Supplementary Figure 8. Band structures and density of states calculated using PBE methods.

REFERENCES

[1] B. Mortazavi, E. V. Podryabinkin, I. S. Novikov, et al., Accelerating first-principles estimation of thermal conductivity by machine-learning interatomic potentials: A MTP/ShengBTE solution, Computer Physics Communications 258, 107583 (2021).
tion of thermal conductivity by machine-learning interatomic potentials: A MTP/ShengBTE solution, Computer Physics Communications 258, 107583 (2021).
[2] W.-X. Zhou, C.-W. Wu, H.-R. Cao, Y.-J. Zeng, G. Xie, and G. Zhang, Abnormal thermal conductivity increase in β-Ga2O3 by an unconventional bonding mechanism using machine-learning potential, Materials Today Physics 52, 101677 (2025).
[3] J. Lü, F. Xu, Y. Zhou, X. Mo, Y. Ouyang, and X. Tao, Four-phonon enhanced the thermoelec-
tric properties of ScSX (X = Cl, Br, and I) monolayers, ACS Applied Materials & Interfaces 16, 24734 (2024).
[4] D. A. Muller, Free electron gas in 2d and 1d, MSE 5470 Lecture Notes, Cornell University (2003), [Online; accessed 15-Aug-2025].
[5] M. Jonson and G. D. Mahan, Mott's formula for the thermopower and the wiedemann-franz law, Phys. Rev. B 21, 4223 (1980).